Laser-only AO, readout noise studies and AO verification and integration for ELTs

Alastair Basden,[a] Nigel Dipper,[a] Eric Gendron,[b] Damien Gratadour,[b] Zoltan Hubert[b], Tim Morris,[a] Richard Myers,[a] Gerard Rousset,[b] Arnaud Sevin[b], Fabrice Vidal,[b] Angus Wilson[a]

[a]Department of Phyics, Durham University, South Road, Durham, DH1 3LE, UK. [b] Observatoire de Paris, 61 Avenue de l'Observatoire, 75014 Paris, France.

ABSTRACT

We present a concept for visible near-diffraction limited lucky imaging with full-sky laser assisted adaptive optics. Simulation results are given, along with first on-sky measurements taken with the CANARY AO system on the William Herschel Telescope, and extension to ELT scales.

We also present a study of readout noise in EMCCD and sCMOS detectors, with findings that are perhaps surprising when compared with naive models of sCMOS noise. We discuss the relative trade-offs of these detectors for ELT-scale AO and lucky imaging.

Finally we introduce the concept of real-time simulation, necessary for integration and verification of ELT-scale AO systems, and provide details of the system developed for CANARY.

1. INTRODUCTION

Adaptive optics (AO)[1] is a widely accepted technology on large telescopes, using wavefront sensor information to actively compensate for atmospheric seeing. Many different types of AO systems have been commissioned, including single conjugate AO (SCAO), multi-conjugate adaptive optics (MCAO), ground layer AO (GLAO), multi-object AO (MOAO), laser tomographic AO (LTAO) and eXtreme AO (XAO). However all of these systems suffer from a lack of sky coverage, since bright guide stars are required, even when laser guide stars (LGSs) are used, and these bright stars cannot be found at every location in the sky. Additionally, AO correction at visible wavelengths is usually poor (with the exception of XAO systems).

1.1 Lucky imaging

The lucky imaging concept[2] involves capturing short exposure images (with 10 ms typical exposure times), and selecting the best of these for integration to create a final image, typically using a shift-and-add technique. Lucky imaging relies of using the rare moments when atmospheric perturbations are minimal, and enables near-diffraction-limited images at visible wavelengths to be captured. This concept has seen some success in astronomy on small 1–2 m class telescopes, but is not yet widely used, particularly on larger telescopes where the probability of capturing a good (or "lucky") image becomes tiny. Some astronomers are also not keen on this technique since there is a perceived wastage of light in the image frames that are discarded.

In these proceedings, we introduce a concept for tomographic AO assisted lucky imaging,[3] where the sky coverage for the AO system is unlimited, relying only on LGSs. By using multiple LGSs, a tomographic wavefront reconstruction can be carried out, allowing a GLAO correction to be performed over a wide field of view, or a LTAO correction offering improved correction over a smaller field. A lack of natural guide stars (NGSs) will mean that the corrected images are not fixed within the focal plane. However, utilising the lucky imaging technique means that these images can then be shifted to a common position before co-addition. The use of AO correction will greatly increase the probability of obtaining a lucky image. Simulation and on-sky results are presented, obtained using the CANARY AO demonstrator instrument.[4]

Further author information: (Send correspondence to Alastair Basden)
Alastair Basden: E-mail: a.g.basden (a t) durham.ac.uk, Telephone: +44 191 3342229

1.2 Detector readout noise modelling

AO and lucky imaging both rely on low noise detectors, typically either electron multiplying CCDs (EMCCDs) or scientific CMOS (sCMOS) cameras, and the readout noise associated with the chosen detector can have a large impact on AO performance. Here we present results of a study performed comparing different readout noise models.[5]

EMCCDs are CCD detectors capable of imaging at very low light levels, with effective sub-electron readout noise obtained using an on-chip gain mechanism. However, this mechanism is stochastic which introduces uncertainty in the recorded output. The quantum efficiency (QE) of these detectors can reach above 90%, i.e. 90% of incident photons are converted into a detected signal.

sCMOS detectors are low noise CMOS imagers, with root-mean-square (RMS) readout noise levels approaching one photo-electron. However, due to the nature of the technology, each pixel has its own readout electronics, and therefore the RMS readout noise varies from pixel to pixel following a log-normal probability distribution, with significant numbers of pixels having higher readout noise. The QE of these detectors can be up to 80%.

1.3 Real-time simulation for AO integration and verification

Extensive numerical simulation and modelling is usually involved in the design process of an AO system. This is a time consuming process, and for large telescopes, the simulations run far slower than real-time. When the AO system design has been completed, and the system built, verification and integration with telescope facilities is required, followed by final commissioning. However, for Extremely Large Telescope (ELT)-scale systems, the AO systems will be dependent on components such as deformable mirrors (DMs) and LGSs which are integrated with the telescope structure, and therefore cannot be used during laboratory testing due to size and cost of these components. Likewise, state-of-the-art components such as wavefront sensors cannot also be replicated to all the laboratories where AO system testing and verification will be carried out.

The solution is to use a real-time hardware-in-the-loop simulation capability[6] to allow high fidelity modelling of components that are not physically present, during integration and verification. We here provide an example of the use of this real-time simulation concept in the CANARY AO instrument.

1.4 Summary of proceedings

In these proceedings, we will first discuss the AO-assisted lucky imaging concept and provide results in §2. In §3 we present results related to models of detector readout noise. In §4 our real-time simulation concept is discussed along with its application to CANARY, and we conclude in §5.

2. LGS AO ASSISTED LUCKY IMAGING

The concept for LGS assisted lucky imaging is suitable for use with all forms of tomographic AO, allowing the telescope size applicable for lucky imaging to be increased, and a schematic diagram for this concept is shown in Fig. 1.

Although the AO correction achieves full sky coverage, natural guide stars are still required by the lucky imaging instrument. We have previously calculated[3] that sources with I-band magnitudes of 18 or brighter are required to allow image selection and recentering during lucky image processing on a 4 m class telescope, with fainter targets being usable on larger telescopes. At this brightness, near full-sky-coverage is achieved, with only very limited areas of the sky not having a suitable guide star.

The ability to reach magnitudes as faint as this for lucky imaging, which are not generally achievable for AO systems, is due to several facts:

1. Full telescope aperture used for light collection, rather than division into sub-apertures.
2. Lower frame rate can be used as there is no closed-loop correction.

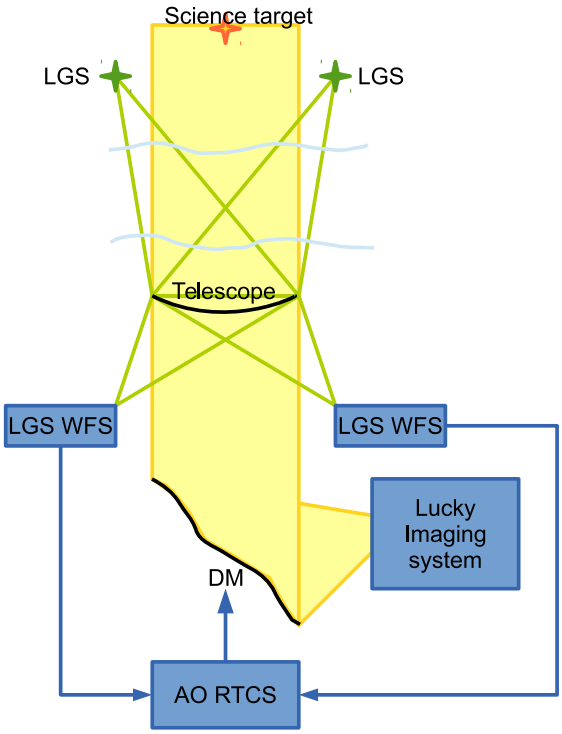

Figure 1. A figure showing the LGS AO assisted lucky imaging technique. Tomographic wavefront correction is performed using LGS information, and selected short exposure images are then combined to provide a high quality PSF.

2.1 Simulations of LGS AO assisted lucky imaging

We have used Durham AO simulation platform (DASP)[7] to model performance of LGS AO assisted lucky imaging.[3] These models included 4 Rayleigh LGS on a 4.2 m telescope, with a 22" radius asterism (i.e. the LGS were positioned on a 22" radius circle). We assumed 8×8 sub-apertures and a 9×9 actuator DM, with the AO system operating at 200 Hz. The lucky imaging frame rate was 100 Hz, and the lucky imaging wavelength was taken as 800 nm (I-band).

2.2 Main results and conclusions for lucky imaging behind tomographic AO

Fig. 2 shows predicted Strehl ratio as a function of fraction of lucky imaging frames selected (with 100% being pure shift and add), for different image selection metrics, based on Strehl, point spread function (PSF) diameter, and residual tomographic wavefront error. It is unsurprising that selection by Strehl ratio gives best performance, since this is directly related to the performance metric. However, it should be noted that using an image based metric of PSF width gives similar performance as a wavefront sensor (WFS) based metric. This is promising because it will allow selection based on WFS measurements, allowing fainter lucky guide stars to be used only for image centring.

Fig. 3 shows predicted Strehl as a function of fraction of lucky imaging frames selected for different atmospheric conditions, with both static and variable seeing. We note here that the ability to model variable seeing is crucial for lucky imaging modelling, since the lucky imaging technique relies on having periods when the atmosphere is well behaved. The difference in performance between cases with a static r_0 of 15 cm, and with r_0 varying between 10–20 cm (with a mean of 15 cm) is clearly evident when frame selection percentage is below about 50%: In this case, the best frames are being selected.

Fig. 4 shows predicted Strehl as a function of off-axis distance, i.e. gives a representative field of view. It can be seen that the resulting I-band combined images maintain reasonable performance up to 20 arcseconds off-axis, with small improvements beyond this. We note that this corresponds well with the LGS asterism diameter, with

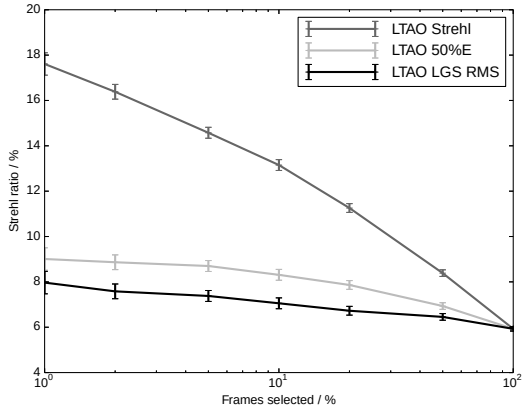

Figure 2. A figure showing I-band Strehl ratio as a function frame selection fraction. The selection metric is given in the legend.

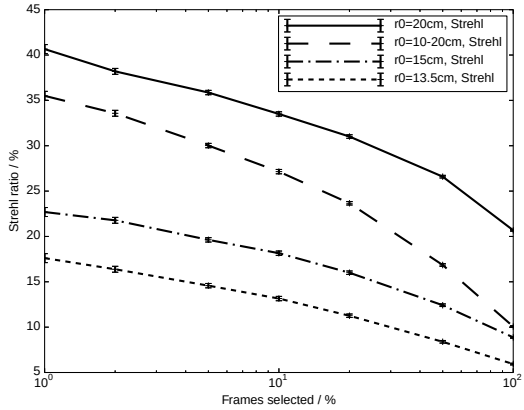

Figure 3. A figure showing I-band Strehl as a function of image selection fraction for different atmospheric conditions as given in the legend. For the variable seeing case, the seeing varies sinusoidally between the minimum and maximum.

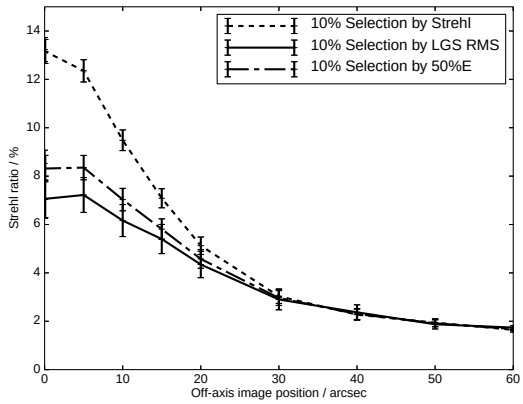

Figure 4. A figure showing I-band Strehl as a function of off-axis distance for a image selection fraction of 10%.

LTAO correction performed. If the LGS asterism diameter is increased, we would expect better performance at wider fields though a reduced performance close to on-axis, due to the lower performance from the AO system.

2.3 On-sky results

Using the CANARY AO demonstrator instrument on the William Herschel Telescope, we investigated LGS-assisted lucky imaging. The AO system was operating at 150 Hz, with the LGS height at 15 km. Although we did not have an optical imager, we used K-band images with a 0.1 s exposure, which is equivalent to a 25 ms exposure at 700 nm (in terms of atmospheric behavious), so largely representative of performance achievable using a visible lucky imaging instrument. This was the first tomographic LGS AO performed on-sky without a requirement for a NGS.

Results are shown in Fig. 5, comparing results for a traditional long exposure image, a shift and add image (100% selection), and lucky imaging with 10% selection. Within this figure, cases for no AO correction, full AO correction (LGS and NGS), and for LGS-only AO correction are shown. In the AO corrected cases, the diffraction ring is clearly visible, when lucky imaging is used, though not present in long exposure images. With 10% frame selection and LGS-only AO, a full-width at half-maximum (FWHM) of 108 mas is achieved (with the diffraction limit being 105 mas). In these cases, the image selection criteria is based on Strehl ratio. However, correction by wavefront error also showed some promise.

3. LOW NOISE DETECTOR READOUT MODELS

The readout noise of a CCD is determined by the that of the readout register port (or ports for multi-port devices). This means that every pixel (per readout port) has the same readout noise characteristics (with the exception of some edge pixels, depending on controller design), and therefore, a CCD can be well characterised by a single (per readout port) readout noise RMS value. An sCMOS detector on the other hand has an individual readout port for each pixel, and therefore, a different RMS readout noise value for each pixel. The distribution of RMS readout noise is found to follow a distribution that is approximately log-normal, though a more accurate fit is given in,[5] and shown in Fig. 6.

We have investigated the effect of readout noise models on Shack-Hartmann wavefront sensor accuracy, using a Monte-Carlo technique, concentrating on a single sub-aperture. Our method is as follows:

1. A sub-aperture spot at a random location is generated (noiseless), and true centre of gravity computed.
2. Noise (shot and readout) is added to the image.
3. The noisy spot position is determined using a centre of gravity.

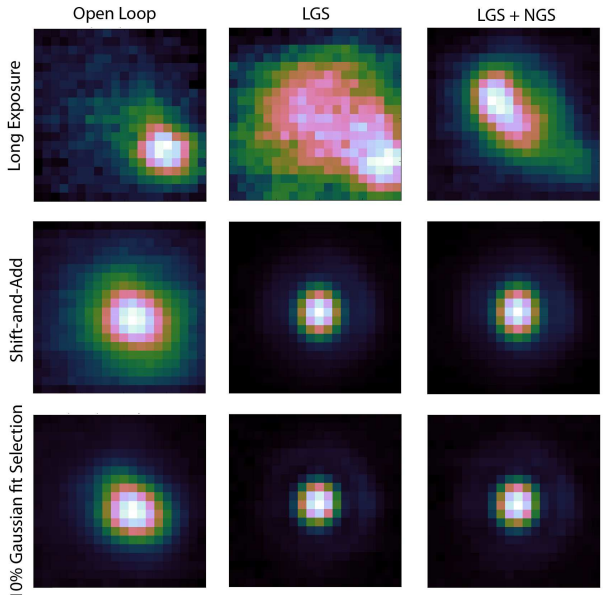

Figure 5. A figure showing on-sky LGS assisted lucky imaging performance obtained with CANARY. Images are K-band with a 0.1 s exposure time (equivalent to 25 ms at 700nm). From top to bottom, shows no lucky imaging, shift-and-add (100% selection) and 10% selection. From left to right are shown open-loop (no AO correction), LGS-only AO, and LGS+NGS AO correction. The selection metric for images is width of a Gaussian fit.

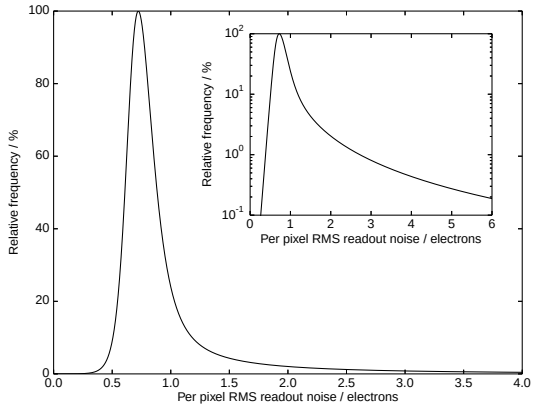

Figure 6. A figure showing a fit to manufacturer sCMOS readout noise statistics. Readout noise verses probability is shown.

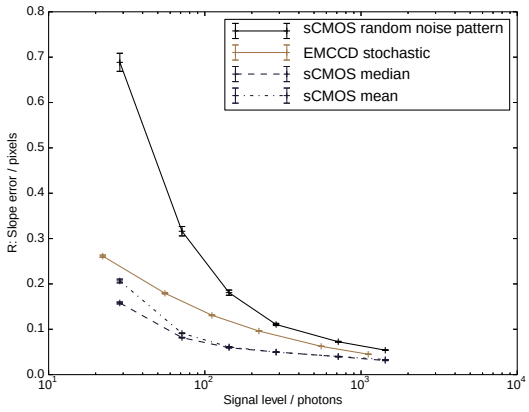

Figure 7. A figure showing predicted wavefront slope error as a function of signal level for different detector readout noise models for a 16×16 sub-aperture. A QE of 70% is assumed for the sCMOS, and 90% for the EMCCD.

4. The distance (in pixels) between noiseless position and noisy estimate is computed.

5. This process is repeated many times and the mean distance returned as the performance metric, or slope error.

A range of sub-aperture sizes, spot sizes and flux levels have been investigated.

3.1 Key results from detector readout models

Fig. 7 shows slope error as a function of signal level for different detector readout noise models. It can be seen that when using the mean or median quoted value for sCMOS readout noise, performance is better than for an EMCCD. This is primarily due to the stochastic gain mechanism of the EMCCD which effectively halves the quantum efficiency: here we have simulated this mechanism fully using a Monte-Carlo method. However, when a full model of sCMOS readout noise is used, including the variation in RMS noise for different pixels, performance predicted for an sCMOS detector is significantly worse at lower light levels. It is therefore recommended that sCMOS detectors are to be used in AO instrumentation, a study including an accurate readout noise model should be performed for the instrument in question. It should be noted that since the readout noise of individual pixels will be known for any given detector, in the case of large sub-apertures it may be possible to mask out high noise pixels and thus improve performance (or otherwise take them into account, for example using a matched filter algorithm). However, we have not considered this here.

4. REAL-TIME SIMULATION FOR CANARY

Being an AO on-sky test-bench, the CANARY instrument regularly undergoes design changes as new components are added, and new features are tested. This, combined with short commissioning periods, and few nights on-sky means that it is beneficial to be able to test, verify and develop tools and graphical interfaces without physical hardware present. For this purpose, we have developed a real-time simulation tool based on DASP. The concept is simple: rather than connecting the CANARY real-time control system (RTCS) to physical WFSs and DMs, we instead connect it to simulated ones. Within the simulation, we include a model of the atmosphere, the telescope and the CANARY optical bench, so that data generated and passed to the RTCS appears in a similar format to that obtained using physical components. In particular, we take care with relative WFS and DM rotations, and with the WFS pixel scales and the allowable DM stroke and surface scale. Fig. 8 shows a screen shot of the simulation configuration tool for this simulation.

With this real-time simulation capability, we are able to switch the RTCS freely from simulation to on-sky mode. The simulation representation is close enough to allow us to use control matrices generated in simulation on-sky, though with reduced performance (due to static aberrations, and since the simulation is not a true

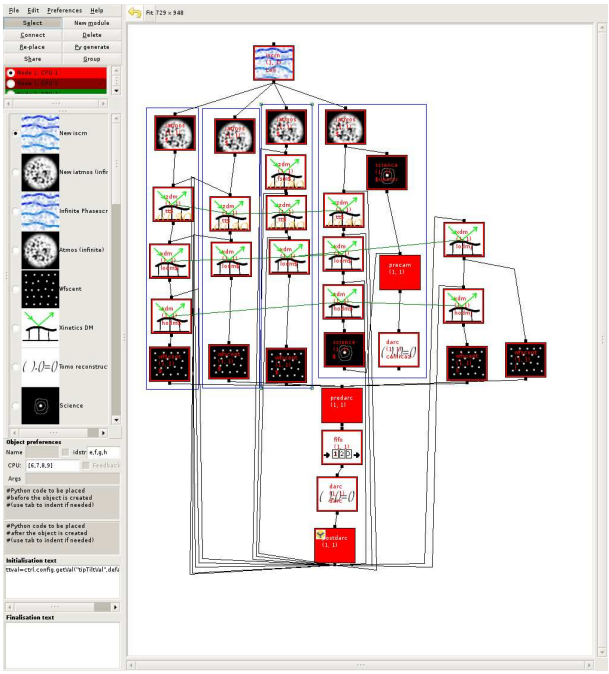

Figure 8. A screenshot of the DASP simulation configuration tool showing the CANARY real-time simulation configuration. Blue boxes repeat their contents a number of times (i.e. there are multiple wavefront sensors repeated).

representation of the optical setup, for example small misalignments, etc). This provides the opportunity to fully test and debug software from several locations simultaneously, without requiring on-sky operation: our real-time control system is CPU-based, and therefore can be operated with non-specific hardware when in simulation mode, i.e. when interfaces to physical cameras and DMs are not required.

The simulation is scalable across multiple computing nodes using MPI. However, to reduce complexity, our CANARY simulation is typically operated on a single node. Frame rates of typically 30 Hz are achieved, i.e. not true real-time (150 Hz), though fast enough to enable a user to operate the system responsively without introducing significant delays. We note that the term real-time simulation refers more to the combination of a real-time control system with a simulation, rather than operation at real-time rates, though of course this should always be a goal.

The use of this real-time simulation capability has enabled us to implement advanced features such as update of correlation reference images during closed-loop operation[8] which would otherwise have required significant (unobtainable) on-sky commissioning time. A study of novel wavefront reconstruction strategies was also enabled using this real-time simulation concept.

We therefore highly recommend this approach for future AO systems, given the potential for significantly reduced AO integration, verification and commissioning times.

5. CONCLUSIONS

We have presented three concepts for AO, along with results that we have obtained. A LGS-only AO concept has been detailed, which has the potential to provide near-diffraction limited visible wavelength imaging when combined with lucky imaging, with near full sky coverage. A study of low noise detector readout models has been made with the conclusion that AO system designers must pay attention to readout noise models when investigating AO performance with sCMOS detectors. Finally, the real-time simulation concept used by CANARY has been detailed, along with examples of how CANARY has benefited.

REFERENCES

[1] Babcock, H. W., "The Possibility of Compensating Astronomical Seeing," *Pub. Astron. Soc. Pacific* **65**, 229–+ (Oct. 1953).

[2] Fried, D. L., "Probability of getting a lucky short-exposure image through turbulence," *Journal of the Optical Society of America (1917-1983)* **68**, 1651–1658 (Dec. 1978).

[3] Basden, A. G., "Visible near-diffraction limited lucky imaging with full-sky laser assisted adaptive optics," *MNRAS* **442**, 1142–1150 (2014).

[4] Myers, R. M., Hubert, Z., Morris, T. J., Gendron, E., Dipper, N. A., Kellerer, A., Goodsell, S. J., Rousset, G., Younger, E., Marteaud, M., Basden, A. G., Chemla, F., Guzman, C. D., Fusco, T., Geng, D., Le Roux, B., Harrison, M. A., Longmore, A. J., Young, L. K., Vidal, F., and Greenaway, A. H., "CANARY: the on-sky NGS/LGS MOAO demonstrator for EAGLE," in [*Society of Photo-Optical Instrumentation Engineers (SPIE) Conference Series*], *Society of Photo-Optical Instrumentation Engineers (SPIE) Conference Series* **7015**, 0 (July 2008).

[5] Basden, A., "Analysis of electron multiplying charge coupled device and scientific CMOS readout noise models for ShackHartmann wavefront sensor accuracy," *JATIS* **1(3)**, 039002–1 – 039002–10 (July 2015).

[6] Basden, A., "A real-time simulation facility for astronomical adaptive optics," *MNRAS* **439**, 2854–2862 (Feb. 2014).

[7] Basden, A. G., Butterley, T., Myers, R. M., and Wilson, R. W., "Durham extremely large telescope adaptive optics simulation platform," *Appl. Optics* **46**, 1089–1098 (Mar. 2007).

[8] Basden, A. G., Chemla, F., Dipper, N., Gendron, E., Henry, D., Morris, T., Rousset, G., and Vidal, F., "Real-time correlation reference update for astronomical adaptive optics," *MNRAS* **439**, 968–976 (Mar. 2014).